Journal of Materials Chemistry A

Accepted Manuscript

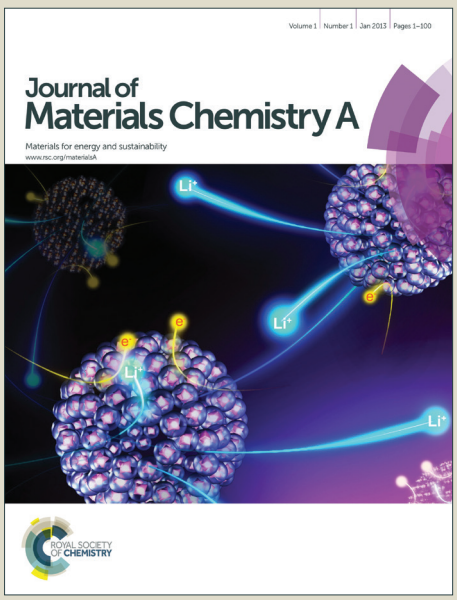

ROYAL SOCIETY OF CHEMISTRY

www.rsc.org/materialsA

Enhanced Reactive Adsorption of H_2S on Cu-BTC/ S- and N- Doped GO Composites

by

Amani M. Ebrahim[1], Jacek Jagiello[2] and Teresa J. Bandosz[1*]

[1] Department of Chemistry,
[1]The City College of New York
160 Convent Ave
New York, NY 10031

[2] Micrometrics Instrument Corporation
Norcross, GA 30093 (USA)

*Whom correspondence should be addressed to: Tel: (212)650-6017; Fax: (212)650-6107; E-mail: tbandosz@ccny.cuny.edu

Abstract

New composites containing Cu-BTC and S- and N- doped graphite oxides (GOs) were synthesized. The composites were evaluated as adsorbents of H_2S at ambient conditions. The texture and chemistry of the initial samples and those exposed to H_2S were analyzed using a wide range of analytical techniques (XRD, SEM-EDX, FTIR, thermal analysis-MS, and nitrogen adsorption). The performance of the new composites as H_2S adsorbents was much better than that of the parent MOFs. It was owing to formation of new microporosity as a result of linkages between the sulfonic acids and amine groups of modified GO and copper centers Cu-BTC. The presence of moisture in the pore system increased the amount adsorbed. Physical adsorption and reactive adsorption play an important role in the mechanism of retention. The removal of H_2S is favored on the composites with higher surface heterogeneity, which facilitates retention of H_2S molecules mostly in the form of sulfides. Given the differences in the chemistry of the N- and S- containing groups in the composites, distinct mechanisms of adsorption occur, which result in sulfides/sulfates of unique morphologies. Nitrogen functional groups catalyze the formation of superoxide ions on the graphene phase, resulting in the partial oxidation of H_2S and in the release of SO_2

Keywords: MOF-graphite oxide composites, reactive adsorption, hydrogen sulfide, porosity, surface chemistry

Introduction

Hydrogen sulfide is a toxic, corrosive gas that is a byproduct of several industrial synthesis (ex. carbon disulfide production) processes and mining activities. It is one of the main causes of environmental pollution. The main anthropological source of H_2S emission is in the natural gas refineries. Release of H_2S to the environment, particularly to ambient air affects its in detrimental ways. Gas purification techniques are emphasized to resolve the challenges addressing air pollution. Small molecules such as H_2S, which are not strongly retained on the surface of adsorbents require separation media with highly polar/hydrophilic surface features, which can induce reactive adsorption via hydrogen bonding, complexion and acid-base reactions, or media promoting redox reaction leading to hydrogen sulfide oxidation. [1, 2,3, 4]

The micropores nature of Metal Organic Frameworks (MOFs) and their tunable pore sizes encourage their usage in gas adsorption, catalysis, separation and purification. [5,6] Nevertheless, their application is rather limited due to the lack of well-developed chemistry in the form of functional/reactive groups for the retention of adsorbate molecules via reactive adsorption. This directs the attention of the researchers to MOF-GO composites. [7, 8, 9] Published results suggest that in such structures the dense array of carbon atoms in graphite oxide enhances the dispersive interactions and the MOF structure is the main contributor to porosity and reactive centers[10, 11]. Moreover, the specific synergy between two components can lead to the formation of unique adsorption centers. [5] It was shown that the synergistic effects of chemistry and porosity of graphite oxide in MOF/GO composites enhance the performance of these materials as adsorbents of acidic gases such as H_2S, [12] and NO_2 [13] . Surface dispersive forces of MOF/GO

composites were also responsible for a significant improvement in the n-hexane adsorption capabilities. [14] A combination of a high surface area of MOFs and the unique layers of GO showed better adsorption affinity than MOF and GO alone for the separation of organochlorine pesticides. [15]

Recently the composites of Cu-BTC MOF with aminated graphite oxides have been shown as excellent adsorbents of CO_2, at low [16] and high pressure [17]. Following this line of research and the fact that nitrogen species incorporated to graphite oxide resulted in a high degree of heterogeneity and defects in MOF units beneficial for the adsorption process, the objective of this paper is to introduce composites of Cu-BTC with sulfur and nitrogen co-doped GOs as reactive adsorbents of toxic gases. To understand the performance as adsorbents of hydrogen sulfide at ambient conditions the structure and chemistry of these new materials have been extensively analyzed. It is expected that incorporation of heteroatom-based functionalities to GO will affect the structure of MOF units and the structure of the composites itself. [16] Moreover, a significant alteration of surface chemistry is also expected. All of these should affect the adsorptive performance. The chemical and structural heterogeneity of the composites would likely enhance the adsorption of H_2S molecules especially at the MOF/modified GO interface where a new chemistry and porosity is expected to exist. [18]

Experimental

1. Materials

1.1 Synthesis of sulfur and nitrogen co-doped graphite oxide (GO)

Graphite oxide GO was synthesized by the oxidation of graphite following Hummers methods [19] and it was used as a precursor for S-, N- modified GOs.

Sulfanilic acid (SA) modified GO (GOSA) and 4-ammonium polystyrene sulfonate modified GO (GOPSN) were prepared by hydrothermal treatment of GO with corresponding compounds. The details on the modification procedures and materials' characterization are addressed elsewhere [20].

1.2 Synthesis of MOF-S- and N-doped GO composites

The synthesis of the composites was carried out following the procedure described by Petit and coworkers [21] with slight amendments. Briefly, $Cu(NO_3)_2.2.5H_2O$ (5.0 g) and BTC (2.5 g) were stirred in 43 mL of dimethylformamide (DMF) for 0.5 h, the solution was sonicated for 10 minutes. Ethanol (43mL) was added to the mixture and stirred for 0.5 h; the solution was then sonicated for an additional 10 minutes. De-ionized water (43mL) was added to the solution and stirred for 0.5 h and sonicated for 10 minutes. When all the crystals were dissolved a modified GO sample (10 wt.% of parent Cu-BTC) was introduced to the solution and the suspension was stirred for 10 minutes and sonicated for 45 minutes. The mixture was then transferred to a round bottom flask and heated at 94 ^{o}C under shaking for 24 h. The mother liquor was decanted and rinsed with dimethylformamide and then rinsed again with dichlormethane (DCM). The blue crystals were immersed in dichloromethane for 50 h to allow for solvent exchange then filtered twice and replenished with fresh dichloromethane. The crystals were heated at 115 ^{o}C to activate the materials and remove the solvent. The composites are referred to as MOF-GOSA and MOF-GOPSN.

2. Methods

2.1 Adsorption of Nitrogen

Adsorption isotherms of nitrogen at 77 K were measured for these samples using the high-resolution Micromeritics 3Flex instrument equipped with high-vacuum system, three micropore ports and three 0.1 Torr pressure transducers. The samples were degassed under vacuum at 393 K overnight prior to the adsorption measurements.

2.2 Surface pH

The samples were first dried, then a 0.1 g sample of dry adsorbent was added to 5 mL of deionized water, and the suspension was stirred overnight to reach equilibrium. The pH was measured using Fischer scientific, Accumet Basic pH meter.

2.3 SEM/EDX

Scanning electron microscopy (SEM) was performed on Zeiss Supra 55 instrument with a resolution of 5 nm at 30 kV. Analyses were performed on a sample powder previously dried. For some samples, a sputter coating of a thin layer of gold was performed to avoid specimen charging. Electron – dispersive X-ray spectroscopy (EDX) analysis was done at a magnification of 15 KX with an accelerating voltage of 15.00 kV.

2.4 XRD

To obtain crystallographic structure of the materials XRD was employed. Using standard powder diffraction procedures, the adsorbents (fresh and exhausted) were placed in a mount and inserted in the machine; the X-ray diffraction was measured on a Philips X'Pert X-Ray diffractometer using $Cu_{K\alpha}$ radiation with a routine power of 1600 W (40 kV, 40 mA)

2.5 Thermal analysis/ Mass spectroscopy

Thermogravimetric (TG) curves, their derivatives (DTG) and m/z profiles were obtained using a TA Instruments thermal analyzer, Q600, coupled with an Omnistar GSD 320 (Pfeiffer Vacuum) gas analyzer. The samples (initial and exhausted moist and dry) were previously dried in oven at 100 °C to remove moisture and then heated up to 1000 ^{o}C, with a heating rate 10 °C/min under a He flow of 100 mL/min.

2.6 FTIR

Fourier transform infrared (FTIR) spectroscopy was carried out on a Nicolet Magna-IR 830 spectrometer (diamond crystal) using the attenuated total reflectance method. The spectra were generated, collected 32 times and corrected for the background noise. The experiments were done on powdered samples using a diamond crystal.

2.7 H_2S Breakthrough Capacity

Dynamic breakthrough tests were performed at room temperature. In a typical test, a flow of H_2S diluted with air (1000 ppm) went through a fixed bed of adsorbent with a total inlet flow rate of 225 mL/min for H_2S. The adsorbent's bed contained about 2 cm^3 of glass beads well mixed with the amount of adsorbent required to obtain a homogeneous bed with minimum pressure drop. The concentration of H_2S and SO_2 in the outlet gas was measured using an electrochemical sensor (Multi-Gas Monitor RAE system). The adsorption capacity of each adsorbent was calculated in mg per gram of the material by integration of the area above the breakthrough curve. The tests were conducted in both moist (relative humidity R.H. 71.0%) and dry conditions by diluting H_2S with air. The suffixes ED and EM are added to the name of the samples after the exposure to the gas in dry and moist conditions, respectively.

Result and Discussion

S- and N- doped graphite oxides' surface were found as highly heterogeneous from the chemistry point of view[20]. Even though the SA modified GO contains less heteroatoms on the surface than GOPSN, it has more sulfur in sulfonic acids and more nitrogen as amines, which results in its acidic character (pH value 3.70 as opposite to 4.00) for the PSN modified GO. The porosity analysis reveals that GOSA is more porous than GOPSN (82 m^2/g as opposite to 6 m^2/g for the latter sample).

The chemical and structural differences in the modified GOs are expected to reflect on the properties of their composites with Cu-BTC. Since our goal was their application as adsorbents of hydrogen sulfide, the porosity is considered as of paramount importance. The parameters of porous structure calculated from nitrogen adsorption isotherms (Figure 1) are collected in Table 1. As seen, the surface areas of both composites are about 100% higher than that of Cu-BTC. Moreover, the values obtained are about 45% higher than those for composites of Cu-BTC with GO obtained using Hummers [22] and Brodie methods [23] and are 23 % higher than those for MOF/aminated GO composites, reported recently [18]. Even though the surface of MOF-GOPSN is about 20% higher than that of MOF-GOSA, their volumes of micropores are very similar, suggesting a higher degree of structural heterogeneity in the former sample. Adsorption isotherms in a logarithmic scale are shown Figure 1. At low relative pressure the micropores nature of the composites is clearly visible and the composites reveal a higher volume of small pores than does Cu-BTC.

The much higher surface areas of the composites than that of MOF itself are linked to the linkages between the sulfonic and amine groups of GO and the copper centers. Even though the initial porosity of GOPSN is negligible compared to that of GOSA, the exfoliation of the polar graphene-based sheets in the solvents during the composite preparation provides additional ligands for binding with copper. Moreover, the original ligand, BTC acid, can also bond with the amines on the surface of GO layers. All of this is responsible for the development of additional porosity on the interface between the MOF units and the modified GO layers.

The estimated content of elements in the initial composites obtained from EDS analysis is summarized in Table 3. The results are averaged from 6 spots. A decrease in the amount of copper in the composites in comparison with that in MOF is related to an increase in the content of the carbonaceous phase from GO which also contributes to more oxygen present in the sample. Interestingly, a lot of nitrogen is detected with no detection of sulfur. These results are unexpected and are quite opposite to the EDS results found for the modified GO where much more sulfur than nitrogen was detected in the sample. This suggests that sulfonic groups are involved in the formation of linkages between the MOF units and GO layers in the bulk of the materials. A plausible explanation at this stage is that these hypothesized reactions might result in the release of sulfur in the form of sulfur oxides.

The X-Ray diffraction patterns for the composites (Figure 2) show the presence of all peaks characteristic to MOF itself [24]. The higher intensities of these peaks for MOF-

GOSA than for MOF-GOPSN indicate the higher crystallinity level of the MOF component in the former sample. This can explain the higher surface area of the latter sample and the higher degree of heterogeneity of its pore sizes. Defects must have a significant influence on the parameters of the porous structure, as previously reported [16].

The surface morphology of the MOF-GO composites is shown in Figure 3. For MOF-GOSA the sharp edges of the crystals are visible, similar to those for MOF. Nevertheless, significant differences are seen on the surface of the crystals, which show the heterogeneous structure along the embedded modified graphene sheets. Similar morphology was found for MOF/aminated GO composites [16]. In the case of MOF-GO PSN the octahedral shape of MOF crystals is still preserved, but the sharp edges of Cu-BTC crystals are missing and even rounding at the corners is noticed. Moreover, crystals exhibit some holes/cracks. The imperfection in the crystals can be a positive factor, which can improve ability of these composites to adsorb H_2S [16, 18].

Thermal analysis shows the differences in the chemistry of the composites in comparison with that of MOF (Figure 4). Two main peaks are related to the decomposition of organic ligands and the collapse of the MOF units[25] respectively. For MOF-GOSA the positions of the peaks are shifted to lower temperatures and the low temperature shoulder is narrower than those for MOF and MOF-GOPSN, which indicates a lower thermal stability. That low temperature shift can be also related to decomposition of MOF-GO linkages in which sulfonic acid groups were involved. The contribution of these groups on the surface of GOSA was higher than that on GOPSN [20].

FTIR analysis also provides information about the chemistry of the composites (Figure 5). A weak band at 1200 cm^{-1} appears and it is related to the vibrational frequencies of C-N bonds. The band at 670 cm^{-1} increases in intensity and we link it to coordination of the metal cation (Cu^{+}) with nitrogen, sulfur and oxygen[26] in the graphitic layers. A rather weak shoulder is present at the band around 1550 cm^{-1} and it represents the bending vibration of -NH group in the network [27]. The amides are likely those formed in the reactions between COOH from the organic linkers and- NH_2 [28] at the surface of modified GO. Moreover, such entities were detected on the surface of S- and N-doped GO itself [20]. A weak signal appears for the composites around 1210 cm^{-1} and is likely due to the presence of S=O in the form of sulfones [27] and C-N vibrations from the functional groups[27] in the graphitic layers. The bands around 671 and 940 cm^{-1} are sharper and wider for the composites that for Cu-BTC itself, and are representative of the out of plane bending vibrations of 1,3 and 1,4 disubstituted aromatic rings. Characteristic bands for Cu-BTC representing the stretching vibrations of the functional groups in BTC are clearly visible [29]. For example, the band at 1100 cm^{-1} represents the vibration of C-O in COOH. The band around 1400 cm^{-1} is typical for the C=C (sp^2) vibration in an aromatic ring and the overtone vibrations are weakly seen between 1700-2000 cm^{-1}. The asymmetric carbonyl vibration of C=O in COOH is seen around 1650 cm^{-1}. Given the high resonance stabilization of carboxylates (COO^{-}/Cu^{+}), the symmetric vibration of C=O is seen at lower wavenumber (~ 1450 cm^{-1})[30].

H_2S breakthrough curves measured for the composite materials in both dry and moist conditions are presented in Figure 6. The calculated breakthrough capacities and pH values of the samples surface before and after exposure to H_2S in both moist and dry conditions are summarized in Table 2. The results indicate that the composite with GOSA is a better adsorbent than that with GOPSN and the presence of moisture improves the adsorptive performance for both samples. The breakthrough capacities range from 109 mg/g on MOF-GO PSN in dry conditions to 241 mg/g on MOF-GOSA in moist conditions and are about 59 % higher than those reported on MOF (98 mg/g) [31], and more than 17 % and 48 % higher than those on MOF-GO composites (200 mg/g with 5 wt. % GO and 125 mg/g with 9 wt. % GO respectively. [12, 32] They also show a higher adsorption capacity (75 % and 112 % higher) than those reported on nano sized reduced graphite oxides [33], and perform 40% better than SBA-15 supported ZnO nanoparticles. [34] Moreover, our composites also perform much better than coal based (28-95 mg/g), and coconut based (11-112 mg/g) activated carbons whose performance depends on the surface modification process and chemical activation method. [35, 36] Generally, the caustic impregnated activated carbons showed an improvement in the adsorptive performance than the virgin ones indicating the importance of surface chemistry in the reactive adsorption process. [35, 36]

After the first breakthrough point, the H_2S outlet concentration sharply increases, which indicates the fast kinetics of the adsorption process. It is interesting that SO_2 was detected in the outlet gas and its highest concentration was measured on MOF-GOSA in moist conditions (0.6 ppm), indicating the highest degree of H_2S oxidation on this specific

composite. Since SO_2 was not detected in the outlet gas in the case of MOF/GO composite [32] we link its appearance in the case of our composites to the presence of nitrogen which is known as catalyzing formation of superoxide ions when incorporated to the surface of carbonaceous materials. [35, 36] An important factor for the oxidation reactions might be also higher contribution of sulfonic acid in GOSA than in that in GOPSN. These species can catalyze the oxidation of H_2S in the presence of quinones causing the reduction on the latter. [37]

A positive effect of water present in the pore system is also related to its crucial role in H_2S dissociation, which was found as enhancing the reactive adsorption process. [38] Apparently, the presence of moisture is more advantageous in the case of MOF-GOSA that for MOF-GOPSN. For the former samples almost a two-fold increase in the breakthrough capacity is found in moist conditions compared to that in dry conditions. The surface acidity of the composites expressed as an average pH value decreases upon exposure to H_2S, indicating the formation of acidic species.

The amount of H_2S adsorbed on our materials apparently does not follow the differences in the surface areas of our adsorbents (Table 1). Therefore the higher adsorption on MOF-GOSA than that on MOF-GOPSN might be linked to the higher degree of microporosity of the former sample and differences in the surface heterogeneity from both, chemical and structural points of view.

The evidence of strong interactions of the adsorbate with the active sites of the adsorbents is provided by the analysis of the parameters of the porous structure of the exhausted samples (Table 1). After exposure to H_2S in either dry or moist conditions the surface of MOF-GOSA decreases about 83 % and 68 %, respectively. A smaller decrease in the surface area for the sample exposed to H_2S in moist conditions was also found after adsorption of NO_2 on urea modified UiO-66/ UiO-67 where water was acting as a "screening" factor blocking the "corrosive"/reactive gas entrance to the small pores. [28] Interestingly, for MOF-GOPSN the extent of the decrease in the surface area (~82%) is the same after adsorption in both moist and dry conditions. Thus water apparently affects the adsorption of H_2S on our composites differently.

Analysis of the XRD patterns after H_2S adsorption and their comparison to those for the initial composites brings more information about the structural stability of MOF units in our materials (Figure 2). Even though for the both exhausted MOF-GOSA samples some residual crystallinity still exists, the major changes are noticed indicating the collapse of the major part of the MOF component. This supports the observed decrease in the surface area and porosity. Changes in the XRD patterns for MOF-GOPSN ED are attributed to the partial collapse of the MOF framework by direct interactions of copper with adsorbate molecules as supported by weak diffraction peaks, representing crystalline $CuSO_3$, $CuSO_4$, Cu_2S and CuS. On the other hand, adsorption of H_2S from the moist gas on MOF-GOPSN resulted in a partial collapse of the MOF units and the extent of destruction is relatively smaller than that seen for the composite exposed to dry gas. Water is likely to adsorb at the copper centers and at the interface between GO and MOF,

where the polar groups are located, and does not let a direct attack of H_2S on the copper centers. These changes are comparable to those found on the surface of MOF-GOSA EM. The residual crystallinity for the composites is much more noticeable in moist conditions than in dry ones, and supports the screening of the Cu-O nucleation sites by water molecules. The direct attack of H_2S on these sites results in the noticed collapse as seen in dry conditions [12]. Interestingly, the porosity changes do not directly follows the XRD results and the porosity of MOF-GOPSN run in moist conditions is somehow less preserved than that in dry conditions. This suggests that not only the MOF phase but also the modified graphene phase can contribute to the apparent porosity of the composites with the collapsed MOF phase, and it acts as a scaffold.

The surface changes after the exposure to H_2S are clearly visible in the SEM micrographs collected in Figure 3. The rough edges of MOF are not distinguishable anymore, and they are likely hidden beneath agglomerated sphere- and rod-like particles. These particles are linked to the deposition of copper sulfide by reaction of H_2S with metallic centers. Following the XRD analysis, we interpret the new phase visible on the micrographs for MOF-GOPSN exposed to dry H_2S is as copper sulfides formed as a result of dissociation of the Cu-ligand bonds upon direct interactions of H_2S with copper centers. Since the nanospherical and rod-like shapes of the Cu_2S were formerly reported elsewhere [39, 40], this species can be present in the crystalline form. That reduction of copper must be accompanied by some degree of H_2S oxidation either to elemental sulfur or sulfites/sulfates. Interestingly, the morphologies of MOF-GOSA after exposure to dry H_2S differ form those of MOF-GOPSN. For the later composite, irregular and flake like

particles, which we associate with CuS are shown. [41, 42] The crystalline phase of Cu_2S is hardly detected and the release of SO_2 from the surface of MOF-GOSA rather indicates the predominantly oxidizing environment. The differences in morphology of surface reaction products suggest different mechanisms of interactions between H_2S and both composites, and subsequently different preferential sites for the reactive H_2S attack on the composite structure. The size of the deposited particles seem to be around 200 nm, and they are more noticeable on the surfaces of MOF-GOPSN ED, MOF-GOSA ED and MOF-GOSA EM than on that of MOF-GO PSN EM. The species deposited on MOF-GO PSN after adsorption in moist conditions are smaller in comparison to those formed on MOF-GO PSN ED. It happens in spite of more H_2S adsorbed in moist conditions. It suggests that water promotes a higher dispersion of surface reaction products owing to the mobility of the dissociated ions in the liquid phase.

The EDX maps of the elements on the samples' surface after H_2S adsorption are shown in Figures S1-S3 of Supplementary Information. Sulfur species are homogenously dispersed on the surface of the composites. The percentage of sulfur deposited on the composite surface follows the increasing trend in the adsorption capacities with the exception of MOF-GOPSN ED, where (Table 3) 7.4 at% of sulfur was detected, more than that on MOF-GOPSN exposed to hydrogen sulfide in moist conditions (5.5 at%), which exhibited a higher adsorption capacity. This might be related to a continuous oxidation of sulfur species and the release of adsorbed H_2S as SO_2 from MOF-GOPSN EM before the EDX analysis was carried out. The H_2S breakthrough tests suggest the

surface of this sample in moist conditions show more oxidizing power than that in dry ones, which support the enhancing role of water.

The nature of the new species formed upon exposure to H_2S was also evaluated using thermal analysis. The DTG curves in nitrogen are collected in Figure 4. Exposure to H_2S resulted in visible changes in the composites' chemistry. A new feature detected for both samples exposed to H_2S is a new peak with maximum at 220 ^oC and the disappearance of the peaks related to the decomposition of ligands. [12, 31] We link these new peaks to the thermal decomposition of $CuSO_3$ formed on the surface via oxidization of H_2S. [43] The decomposition of copper sulfides is expected to occur around 220 ^oC [12, 44, 45, 46], and is likely overlapped by the thermal profiles for the oxidized counterpart, $CuSO_3$. While the main peak related to the decomposition of MOF structure is at the unchanged position for MOF-GOPSN (~350 ^oC) after H_2S adsorption, for MOF-GOSA ED and EM it is shifted to higher temperature in comparison with the initial sample and the decomposition takes place at the same temperature as that for the former samples. The changes in surface chemistry after experiments run in moist conditions are more pronounced than those in dry ones, which is in agreement with the XRD results analyzed above. A decrease in the intensity of the peak at ~350 ^oC suggests the involvement of a significant amount of copper in the formation of oxy sulfur salts and sulfides. [47,48]

In order to more precisely determine the chemistry of the surface species and identify in which temperature range sulfur is released from our samples, the thermal decomposition products were analyzed with mass spectroscopy. The thermal profiles for m/z 98, 64, m/z

48 and m/z 34, representing H_2SO_4, SO_2, SO and H_2S, respectively, are collected in Figure 8. For the initial samples the decomposition of sulfonic acid and sulfones is seen at about 350 ^oC [49] by the release of SO_2. After exposure to hydrogen sulfide the signals from SO_2 and SO are stronger (smaller multiplication factors) indicating oxidation of hydrogen sulfide to SO_2. In addition to chemisorption, physisorption also occurs as clearly indicated by the signal for H_2S on the m/z profiles. Those signals representing H_2S are stronger in the dry conditions than in the moist conditions. This might support the findings described above that the extent of H_2S oxidation is favorable in moist conditions. Partial sulfidation of the phenolic groups in the graphitic layer could attribute to the formation of this signal. [50] Another reason for an increase in the intensity of H_2S signal with an increase in the temperature might be in a favorable reduction of sulfates by the carbonaceous phase in the absence of water in the system. Since in thermal analysis the weight loss related to the decomposition of MOF predominates, it s rather impossible to distinguish in a quantitative way the amount of H_2S physisorbed and that which undergoes the reactive adsorption on the surface.

To further investigate the nature of the sulfur species, and the role of surface chemistry in the H_2S removal process, the exhausted samples were analyzed using FTIR (Figure 5). The bands associated with S=O and S-O vibrations at 1300 and 1100 cm^{-1} [51], respectively, are more noticeable after the exposure to H_2S in both dry and moist conditions confirming H_2S oxidation process. [52] The intensities of the bands at 1250 cm^{-1} for MOF-GOSA EM increase. And is likely due to the presence of physisorbed H_2S as suggested by the m/z profiles. [53] The interactions of the copper centers with H_2S are

clearly indicated by the broadening of the band at 663 cm^{-1} representative of the Cu-O stretch in the MOF units. [54, 55] These copper species in the form of sulfides/sulfates are formed by the dissociation of the linkers and reaction of the adsorbate with Cu.

New bands appear at 671, 750, 760, 990, 1630 cm^{-1} after exposure to H_2S resulting from copper sulfite/sulfate formation. The band appearing at 600 cm^{-1} has been previously attributed to the Cu-S. [46] The latters bands at 671, 750, 760, 990 cm^{-1} are assigned to the asymmetric deformation of O-S-O, symmetric and asymmetric S-O vibrations. [56, 57] A prominent band at 1230 cm^{-1} related to the SO_3^{2-} vibration is seen for MOF-GOSA ED as a result of the interactions of the oxidized byproduct, SO_2 with the copper centers. [58] The band representative of the S=O stretch is clearly seen for MOF-GOSA between 1307-1326 cm^{-1} after exposure to H_2S in dry conditions and suggests that the Cu/COO^- is replaced with Cu^{+2}/SO_3^{2-} following the collapse of the framework. In moist conditions, a new band at 1700 cm^{-1} appears and is ascribed to $-NH_4^+$. These species is likely formed by the protonation of amine groups as a result of the dissociation of H_2S to HS^- and H^+ in the pore system. The protonated amines react with the adsorbed sulfite/sulfides species to form ammonium sulfite/sulfide. [59]

For the composites exposed to H_2S in the moist conditions, the dissociation of H_2S to H^+ and HS^- can lead to acid-base reaction and the protonation of nitrogen in amines and imide groups. A larger amount of amine species is present in GOSA than in GOPSN [20] and thus they contribute more to the H_2S adsorption process at the interface between the composite layers. MOF-GOSA is rich in free/ accessible –NH groups that reactively

interact with H_2S. [60] The sulfonic/sulfone groups are crucial in the establishment of composites and development of porosity but the results suggest that they do not participate directly in the H_2S retention process.

The extent of surface oxidation is linked to the distinct and unique surface features. The importance of developed porosity for the H_2S adsorptive performance is evident. On one hand the composite functional groups (epoxy, hydroxyl and amino groups) are involved in chemical reactions with H_2S, on the other hand reactions of H_2S and SO_2 with unsaturated Cu^{+2} centers result in the formation of sulfite/sulfides. The higher surface area and more developed porosity are related to the presence of defects and thus more unsaturated Cu^{+2} centers, which become are involved in the H_2S retention mechanism. In both composites oxidation of the surface is observed and the formation of sulfates and sulfites can be seen (Figure 9). Interestingly, during the dynamic test only in the case of MOF-GOPSN ED, SO_2 was not detected in the outlet while for the rest of the composites SO_2 was detected and suggests its formation and release from the surface. The high release of SO_2 from the surface of MOF-GOSA EM seems to be very specific to this composite. Amines, imides and quinonic functional groups in the modified GOs promote surface heterogeneity in the composites and are involved in the H_2S oxidative process.

The ability of our composites to adsorb H_2S is more favored in the moist conditions that in dry ones. The enhanced porosity in the case of MOF-GOPSN provides more space in the composite for water accessibility and the dissolution of H_2S in that pore system, thus more H_2S is retained via dissolution process, than in the dry conditions. In the case of

MOF-GOSA, the higher amount of H_2S adsorbed is related to the developed microporosity and surface heterogeneity. Although the reactions of sulfur ligands with copper are the most important for the retention process, the acid-base reaction of H_2S with amine groups incorporated in the modified GOs could be also contribute to it. The presence of O and N groups as (phenol/amines/imides) groups in those layers promote acid-base reactions and results in the exceptional performance MOF-GO SA as an H_2S adsorbent. The large amount of sulfonic acids and nitrogen groups present in GOSA is responsible for the release of SO_2 by the oxidation of adsorbed H_2S.

Conclusions

The results obtained indicate the importance of multifunctional groups incorporated into graphene layers for the development of efficient adsorbents for the removal of H_2S. The evaluation of the composites as H_2S adsorbents shows the crucial role of a graphene-based phase for the separation process. Moreover, the presence of sulfonic and heterocyclic organic species (amines, aniline and imides groups) in the graphitic layers introduces polar reactive groups with rich surface heterogeneity enhancing the performance of our composites. The composites exhibit well-developed porosity and new surface morphologies. In the presence of moisture the adsorption capacities were higher than those in dry conditions owing to the dissolution and dissociation of H_2S. H_2S is retained mainly in the form of copper/sulfur salts formed by acid-base reactions. The composite with the sulfanilic acid modified graphite oxide phase shows much better performance than other MOF-GO composites reported in literature. The catalyzing effect of the modified graphene phase results in the formation of SO_2. In moist conditions,

water acts as a "screening" factor blocking the direct attack of H_2S/SO_2 on the copper centers, preserving the structure to some degree. H_2S attacks the metallic centers and the copper sulfides are formed.

Acknowledgement

This study was supported by the ARO (US Army Research Office) grant W911NF-10-1-0030 and W911NF-13-1-0225.

Bibliographic References

(1) Feng, W.; Kwon, S.; Borguet, E.; Vidic, R. Adsorption of hydrogen sulfide onto activated carbon fibers: effect of pore structure and surface chemistry. *Environ. Sci. Technol.* 2005, ***39***, 9744-9749.

(2) Xue, Q.; Liu, Y. Removal of minor concentration of H_2S on MDEA-modified SBA-15 for gas purification. *J. Ind. Eng. Chem.* 2012, ***18*** , 169-173.

(3) Zhang, X.; Dou, G.; Wang, Z.; Li, L.; Wang, Y.; Wang, H.; Hao, Z. Selective catalytic oxidation of H_2S over iron oxide supported on alumina-intercalated Laponite clay catalysts. *J. Hazard. Mater.* 2013, **260** , 104-111.

(4) Bineesh, K. V.; Kim, D.-K.; Kim, M.-I. L.; Park, D.-W. Selective catalytic oxidation of H_2S over V_2O_5 supported on TiO_2-pillared clay catalysts in the presence of water and ammonia. *Appl. Clay Sci.* 2011, ***53***, 204-211.

(5) Petit, C.; Bandosz, T. J. Engineering the surface of a new class of adsorbents: Metal–organic framework/graphite oxide composites. *J. Colloid Interface Sci*. http://dx.doi.org/10.1016/j.jcis.2014.08.026.

(6) Gadipelli, S.; Guo, Z. X. Graphene-based materials: Synthesis and gas sorption, storage and separation. *Prog. Mater. Sci.* 2015, ***69***, 1-60.

(7) Zhou, X.; Huang, W.; Shi, J.; Zhao, Z.; Xia, Q.; Li, Y.; Wang, H.; Li, Z. A novel MOF/graphene oxide composite GrO@MIL-101 with high adsorption capacity for acetone. *J. Mater. Chem. A* 2014, ***2***, 4722-4730.

(8) Maryam, J.; Zhaolin, L.; Kian Ping, L. A Graphene Oxide and Copper□Centered Metal Organic Framework Composite as a Tri□Functional Catalyst for HER, OER, and ORR. *Adv. Funct. Mater.* 2013, ***23***, 5363-5372.

(9) Ahmed, I.; Jhung, S. H. Composites of metal–organic frameworks: Preparation and application in adsorption. *Mater. Today* 2014, ***17***, 136-146.

(10) Petit, C.; Bandosz, T. J. MOF-Graphite Oxide Composites: Combining the Uniqueness of Graphene Layers and Metal-Organic Frameworks. *Adv. Mater.* **2009,** *21*, 4753-4757.

(11) Petit, C.; Bandosz, T. J. Enhanced Adsorption of Ammonia on Metal-Organic Framework/Graphite Oxide Composites: Analysis of Surface Interactions. *Adv. Funct. Mater.* **2010,** *20*, 111-118.

(12) Petit, C.; Levasseur, B.; Mendoza, B.; Bandosz, T. J. Reactive adsorption of acidic gases on MOF/graphite oxide composites. *Microporous Mesoporous Mater.* 2012, ***154***, 107-112.

(13) Levasseur, B.; Petit, C.; Bandosz, T. J. Reactive Adsorption of NO_2 on Copper-Based Metal−Organic Framework and Graphite Oxide/Metal−Organic Framework Composites. *ACS Appl. Mater. Interfaces* 2010, ***2***, 3606-3613.

(14) Sun, X.; Xia, Q.; Zhao, Z.; Li, Y.; Li, Z. Synthesis and adsorption performance of MIL-101(Cr)/graphite oxide composites with high capacities of n-hexane. *Chem. Eng. J.* 2014, ***239*** , 226-232.

(15) Zhang, S.; Du, Z.; Li, G. Metal-organic framework-199/graphite oxide hybrid composites coated solid-phase microextraction fibers coupled with gas chromatography for determination of organochlorine pesticides from complicated samples. *Talanta* 2013, ***115***, 32-39.

(16) Zhao, Y.; Seredych, M.; Zhong, Q.; Bandosz, T. J. Superior Performance of Copper Based MOF and Aminated Graphite Oxide Composites as CO_2 Adsorbents at Room Temperature. *ACS Appl. Mater. Interfaces* 2013, ***5***, 4951-4959.

(17) Policicchio, A.; Zhao, Y.; Zhong, Q.; Agostino, R. G.; Bandosz, T. J. Cu-BTC/Aminated Graphite Oxide Composites As High-Efficiency CO_2 Capture Media. *ACS Appl. Mater. Interfaces* 2013, ***6***, 101-108.

(18) Zhao, Y.; Seredych, M.; Zhong, Q.; Bandosz, T. J. Aminated graphite oxides and their composites with copper-based metal-organic framework: in search for efficient media for CO_2 sequestration. *RSC Advances* 2013, ***3***, 9932-9941.

(19) Hummers, W. S.; Offeman, R. E. Preparation of Graphitic Oxide. *J. Am. Chem. Soc.* 1958, ***80***, 1339-1339.

(20) Ebrahim, A. M.; Rodríguez-Castellón, E.; Montenegro, J. M.; Bandosz, T. J. Effect of chemical heterogeneity on photoluminescence of graphite oxide treated with S-/N- containing modifiers. *Appl. Surf. Sci.* 2015, ***332***, 272-280

(21) Petit, C.; Mendoza, B.; Bandosz, T. J. Reactive Adsorption of Ammonia on Cu-Based MOF/Graphene Composites. *Langmuir* 2010, ***26***, 15302-15309.

(22) Petit, C.; Burress, J.; Bandosz, T. J. The synthesis and characterization of copper-based metal–organic framework/graphite oxide composites. *Carbon* 2011, ***49***, 563-572.

(23) Bashkova, S.; Bandosz, T. J. Insight into the role of the oxidized graphite precursor on the properties of copper-based MOF/graphite oxide composites. *Microporous Mesoporous Mater.* 2013, ***179***, 205-211.

(24) Decoste, J. B.; Peterson, G. W.; Smith, M. W.; Stone, C. A.; Willis, C. R. Enhanced Stability of Cu-BTC MOF via Perfluorohexane Plasma-Enhanced Chemical Vapor Deposition. *J. Am. Chem. Soc.* 2012, ***134***, 1486-1489.

(25) Grzech, A.; Yang, J.; Dingemans, T. J.; Srinivasan, S.; Magusin, P. C. M. M.; Mulder, F. M. Irreversible High-Temperature Hydrogen Interaction with the Metal Organic Framework $Cu_3(BTC)_2$. *J. Phys. Chem. C* 2011, ***115***, 21521-21525.

(26) Li, F.; Zhang, L.; Evans, D. G.; Duan, X. Structure and surface chemistry of manganese-doped copper-based mixed metal oxides derived from layered double hydroxides. *Colloids Surf., A* 2004, ***244*** , 169-177.

(27) Pavia, D.; Lampman, G.; Kriz, G.; Vyvyan, J. *Introduction to Spectroscopy*; Cengage Learning 2008, 29-32.

(28) Ebrahim, A. M.; Bandosz, T. J. Effect of amine modification on the properties of zirconium–carboxylic acid based materials and their applications as NO_2 adsorbents at ambient conditions. *Microporous Mesoporous Mater.* 2014, ***188***, 149-162.

(29) Bhakta, R. K.; Herberg, J. L.; Jacobs, B.; Highley, A.; Behrens, R.; Ockwig, N. W.; Greathouse, J. A.; Allendorf, M. D. Metal−Organic Frameworks As Templates for Nanoscale $NaAlH_4$. *J. Am. Chem. Soc.* 2009, ***131***, 13198-13199.

(30) Liu, X. M.; Rather, S.-u.; Li, Q.; Lueking, A.; Zhao, Y.; Li, J. Hydrogenation of CuBTC Framework with the Introduction of a PtC Hydrogen Spillover Catalyst. *J. Phys. Chem. C* 2011, ***116***, 3477-3485.

(31) Petit, C.; Bandosz, T. J. Exploring the coordination chemistry of MOF-graphite oxide composites and their applications as adsorbents. *Dalton Trans.* 2012, *41*, 4027-4035.

(32) Petit, C.; Mendoza, B.; Bandosz, T. J. Hydrogen Sulfide Adsorption on MOFs and MOF/Graphite Oxide Composites. *ChemPhysChem* 2010, ***11***, 3678-3684.

(33) Song, H. S.; Park, M. G.; Kwon, S. J.; Yi, K. B.; Croiset, E.; Chen, Z.; Nam, S. C. Hydrogen sulfide adsorption on nano-sized zinc oxide/reduced graphite oxide composite at ambient condition. *Appl. Surf. Sci.* 2013, ***276***, 646-652.

(34) Wang, X.; Sun, T.; Yang, J.; Zhao, L.; Jia, J. Low-temperature H_2S removal from gas streams with SBA-15 supported ZnO nanoparticles. *Chem. Eng. J.* 2008, ***142*****,** 48-55.

(35) Stöhr, B.; Boehm, H. P.; Schlögl, R. Enhancement of the catalytic activity of activated carbons in oxidation reactions by thermal treatment with ammonia or hydrogen cyanide and observation of a superoxide species as a possible intermediate. *Carbon* 1991, ***29***, 707-720.

(36) Strelko, V. V.; Kuts, V. S.; Thrower, P. A. On the mechanism of possible influence of heteroatoms of nitrogen, boron and phosphorus in a carbon matrix on the catalytic activity of carbons in electron transfer reactions. *Carbon* 2000, ***38***, 1499-1503.

(37) Furman, F. M.; Hardy, W. B.; Thelin, J. H. H_2S reducing process for polycyclic endoquinones and partial reduction products thereof. US Pat., 3 109027 A, 1963.

(38) Sitthikhankaew, R.; Chadwick, D.; Assabumrungrat, S.; Laosiripojana, N. Effects of humidity, O_2, and CO_2 on H_2S adsorption onto upgraded and KOH impregnated activated carbons. *Fuel Process. Technol.* 2014, ***124***, 249-257.

(39) Liu, Z. Q.; Huang, W. Y.; Zhang, Y. M.; Tong, Y. X. Facile hydrothermal synthesis of Bi_2S_3 spheres and CuS/Bi_2S_3 composites nanostructures with enhanced visible-light photocatalytic performances. *Crystengcomm* 2012, ***14***, 8261-8267.

(40) Yao, K. S.; Lu, W. W.; Li, X. Y.; Wang, J. J. Ionic liquids-modulated two-phase thermal synthesis of three-dimensional CuS nanostructures. *J. Solid State Chem.* 2012, ***196***, 557-564.

(41) Zou, J.; Zhang, J.; Zhang, B.; Zhao, P.; Huang, K. Low-temperature synthesis of copper sulfide nano-crystals of novel morphologies by hydrothermal process. *Mater. Lett.* 2007, ***61***, 5029-5032.

(42) Nan, Z.; Wang, X.-Y.; Zhao, Z. Formation of various morphologies of copper sulfides by a solvothermal method. *J. Cryst. Growth* 2006, ***295***, 92-96.

(43) Chen, Q.; Wang, Z.; Long, D.; Liu, X.; Zhan, L.; Liang, X.; Qiao, W.; Ling, L. Role of Pore Structure of Activated Carbon Fibers in the Catalytic Oxidation of H_2S. *Ind. Eng. Chem. Res.* 2010, ***49***, 3152-3159.

(44) Jiang, L.; Zhu, Y.-J. Cu_2S nanostructures prepared by Cu-cysteine precursor templated route. *Mater. Lett.* 2009, *63*, 1935-1938.

(45) ter Maat, H.; Hogendoorn, J. A.; Versteeg, G. F. The removal of hydrogen sulfide from gas streams using an aqueous metal sulfate absorbent: Part II. The regeneration of copper sulfide to copper oxide—an experimental study. *Sep. Purif. Technol.* 2005, ***43***, 199-213.

(46) Kim, Y.-Y.; Walsh, D. Metal sulfidenanoparticles synthesized via enzyme treatment of biopolymer stabilized nanosuspensions. *Nanoscale* 2010, ***2***, 240-247.

(47) Godočíková, E.; Baláž, P.; Criado, J. M.; Real, C.; Gock, E. Thermal behaviour of mechanochemically synthesized nanocrystalline CuS. *Thermochim. Acta* 2006, ***440***, 19-22.

(48) Hachimi, A.; Vilcocq, L.; Courson, C.; Kiennemann, A. Study of olivine supported copper sorbents performances in the desulfurization process in link with biomass gasification. *Fuel Process. Technol.* 2014, ***118***, 254-263.

(49) Vyazovkin, S. Thermal Analysis. *Anal. Chem.* 2008, ***80*** , 4301-4316.

(50) Rai Puri, B.; Singh Hazra, R. Carbon-sulphur surface complexes on charcoal. *Carbon* 1971, ***9***, 123-134.

(51) Hajlaoui, F.; Yahyaoui, S.; Naili, H.; Mhiri, T.; Bataille, T. Crystal structure, phase transition and thermal decomposition of a copper (II) sulfate dihydrate containing a chiral organic ammonium cation. *Inorg. Chim. Acta* 2010, ***363***, 691-695.

(52) Jha, M. K.; Van Nguyen, N.; Lee, J.-c.; Jeong, J.; Yoo, J.-M. Adsorption of copper from the sulphate solution of low copper contents using the cationic resin Amberlite IR 120. *J. Hazard. Mater.* 2009, ***164***, 948-953.

(53) Beck, D. D.; White, J. M.; Ratcliffe, C. T. Catalytic reduction of carbon monoxide with hydrogen sulfide. 2. Adsorption of water and hydrogen sulfide on anatase and rutile. *J. Phys. Chem.* 1986, ***90***, 3123-3131.

(54) Kumar, P.; Gusain, M.; Nagarajan, R. Synthesis of $Cu_{1.8}S$ and CuS from Copper-Thiourea Containing Precursors; Anionic (Cl^-, NO_3^-, SO_4^{2-}) Influence on the Product Stoichiometry. *Inorg. Chem.* 2011, ***50***, 3065-3070.

(55) Staszak, K.; Regel-Rosocka, M.; Wieszczycka, K.; Burmistrzak, P. Copper(II) sulphate solutions treatment by solvent extraction with Na-Cyanex 272. *Sep. Purif. Technol.* 2012, ***85***, 183-192.

(56) White, R. L. Variable temperature infrared study of copper sulfate pentahydrate dehydration. *Thermochim. Acta* 2012, ***528***, 58-62.

(57) Fukushi, K.; Aoyama, K.; Yang, C.; Kitadai, N.; Nakashima, S. Surface complexation modeling for sulfate adsorption on ferrihydrite consistent with in situ infrared spectroscopic observations. *Appl. Geochem.* 2013, ***36***, 92-103.

(58) Siriwardane, R. V.; Poston Jr, J. A.; Fisher, E. P.; Shen, M.-S.; Miltz, A. L. Decomposition of the sulfates of copper, iron (II), iron (III), nickel, and zinc: XPS, SEM, DRIFTS, XRD, and TGA study. *Appl. Surf. Sci.* 1999, ***152***, 219-236.

(59) Fan, L.; Wu, P.; Zhang, J.; Gao, S.; Wang, L.; Li, M.; Sha, M.; Xie, W.; Nie, M. Synthesis and anticoagulant activity of the quaternary ammonium chitosan sulfates. *Int. J. Biol. Macromol.* 2012, ***50***, 31-37.

(60) Kreulen, H.; Smolders, C. A.; Versteeg, G. F.; Swaaij, W. P. M. Selective removal of H_2S from sour gases with microporous membranes. Part II. A liquid membrane of water-free tertiary amines. *J. Membr. Sci.* 1993, ***82***, 185-197.

Captions to Figures

Figure 1. Nitrogen adsorption isotherms (log scale) for Cu-BTC and composites

Figure 2. XRD patterns for the initial composites and those exposed to H_2S.

Figure 3. SEM micrographs for Cu-BTC and the initial composites and those exposed to H_2S.

Figure 4. TG and DTG curves in nitrogen for the initial composites and those exposed to H_2S .

Figure 5. FTIR spectra for the initial composites and those exposed to H_2S.

Figure 6. H_2S breakthrough curves for the composites measured in moist and dry conditions.

Figure 7. m/z thermal profiles for initial MOF-GOPSN (A) and MOF-GOSA (B) and the exhausted samples.

Captions to Tables

Table 1. Parameters of the porous structure derived from the nitrogen adsorption isotherms for the composites.

Table 2. H_2S breakthrough capacities in moist (EM) and dry (ED) conditions, maximum SO_2 concentration and pH values before and after the exposure to H_2S. [a,b] The capacities of MOF/GO EM are obtained from ref [12] and [31].

Table 3. Contents of elements in atomic % determined from EDS measurements.

Table 1. Parameters of the porous structure derived from the nitrogen adsorption isotherms for the parent MOF and its composites with GO.

Sample	S_{BET} (m^2/g)	V_{mic} (cm^3/g)	V_{tot} (cm^3/g)	V_{mic}/V_t (%)
Cu-BTC	1040	0.445	0.514	87
MOF-GOPSN	1722	0.581	0.682	85
MOF-GOPSN ED	309	0.063	0.254	25
MOF-GOPSN EM	314	0.029	0.395	7
MOF-GOSA	1419	0.554	0.583	95
MOF-GOSA ED	234	0.089	0.169	53
MOF-GOSA EM	447	0.145	0.190	76

Table 2. H_2S breakthrough capacities in moist (EM) and dry (ED) conditions, maximum SO_2 concentration and pH values before and after the exposure to H_2S. [a,b] The capacities of MOF/GO EM are obtained from ref [12] and [31]. They were measured at the same conditions as those used to evaluate the composite samples.

Samples	H_2S Breakthrough capacity	H_2S Breakthrough capacity	Outlet SO_2 Concentration	pH	
	(mg/g)	(mmol/g)	ppm		
				Initial	Spent
MOF/GO EM [a,b]	130	3.66			
MOF-GOPSN ED	109±4.06	3.19±0.2	----	4.30	4.03
MOF-GOPSN EM	125±2.17	3.66±0.06	0.1		3.46
MOF-GOSA ED	133± 5.22	3.90±0.153	0.2	4.33	2.95
MOF-GOSA EM	241± 6.44	7.06±0.188	0.6		2.85

Table 3. Content of elements in atomic % determined from EDS measurements

Sample	Cu	C	O	N	S
Cu-BTC	14.5±2.11	55.5±4.56	26.5±2.41	_	_
MOF-GOSA	8.85±2.50	66.3±7.06	16.3±0.81	6.7±1.97	0.0±0.1
MOF-GOSAED	16.3±4.83	49.0±5.03	22.5±2.52	4.1±0.95	7.3± 1.7
MOF-GOSA EM	16.8±2.42	47.1±1.67	15.0±1.41	2.9±0.85	13.3±3.4
MOF-GOPSN	6.21±2.23	65.5±3.27	20.0±1.61	6.2±1.18	0.0
MOF-GOPSN ED	10.0±1.25	60.8±4.10	16.1±2.04	4.0±1.38	7.4±2.35
MOF-GOPSN EM	10.7±3.04	60.7±2.53	16.3±1.64	4.3±0.71	5.5±1.29

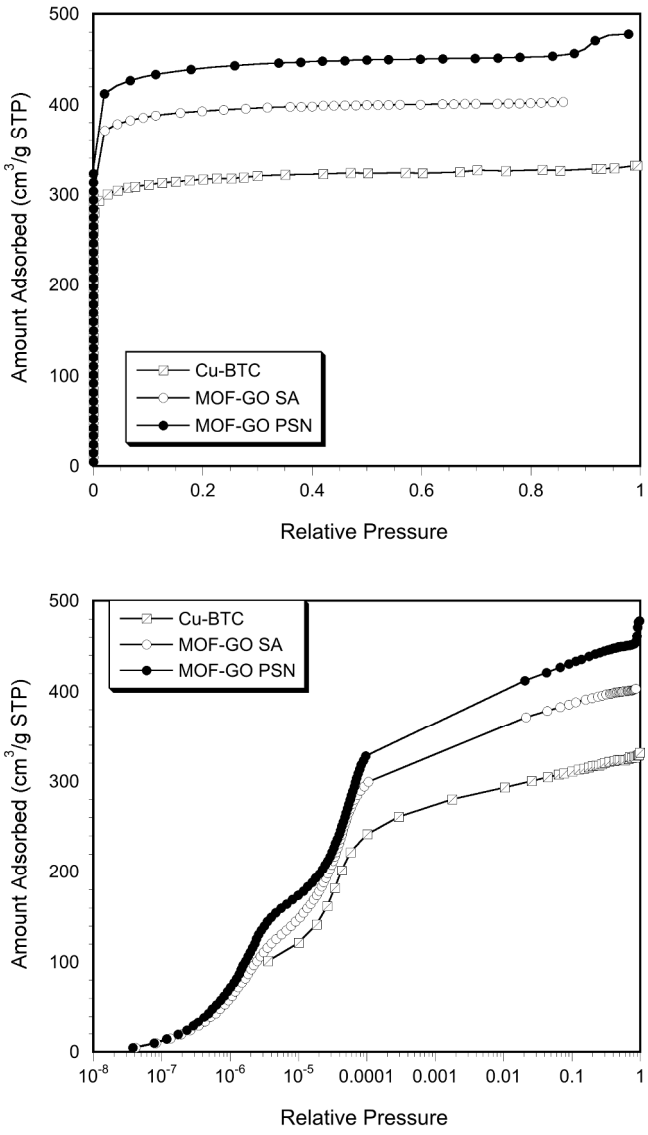

Figure 1.

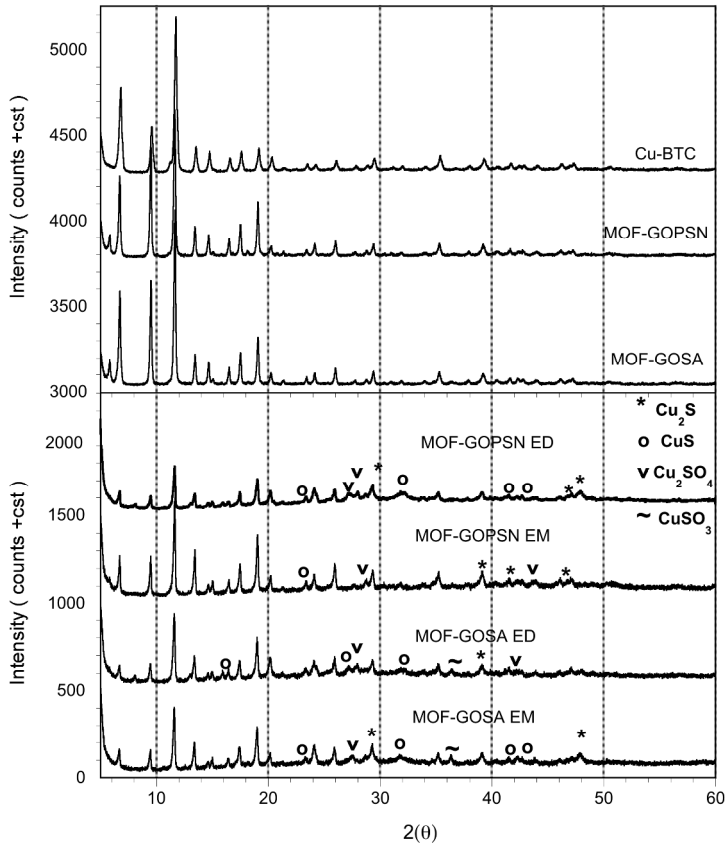

Figure 2.

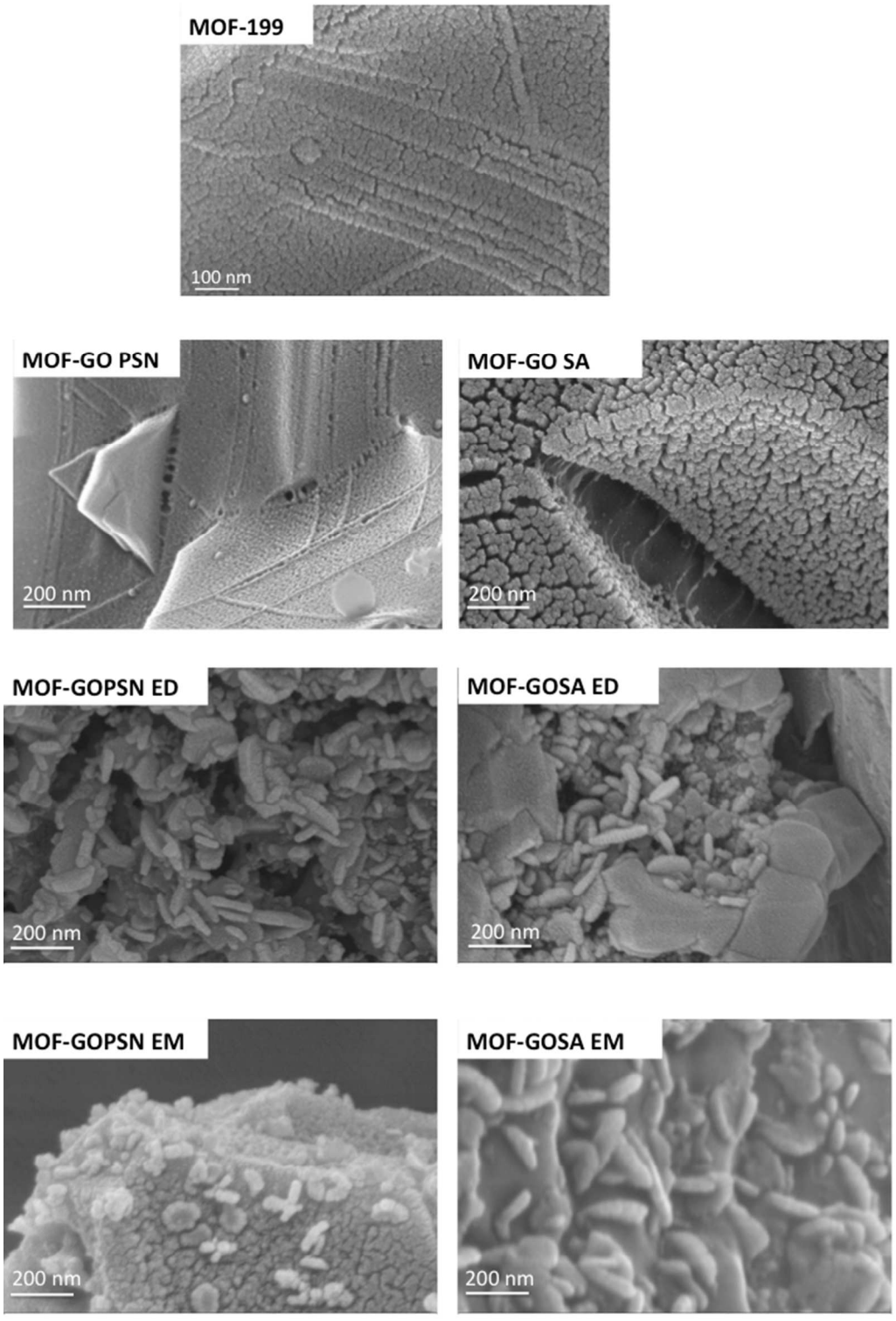

Figure 3.

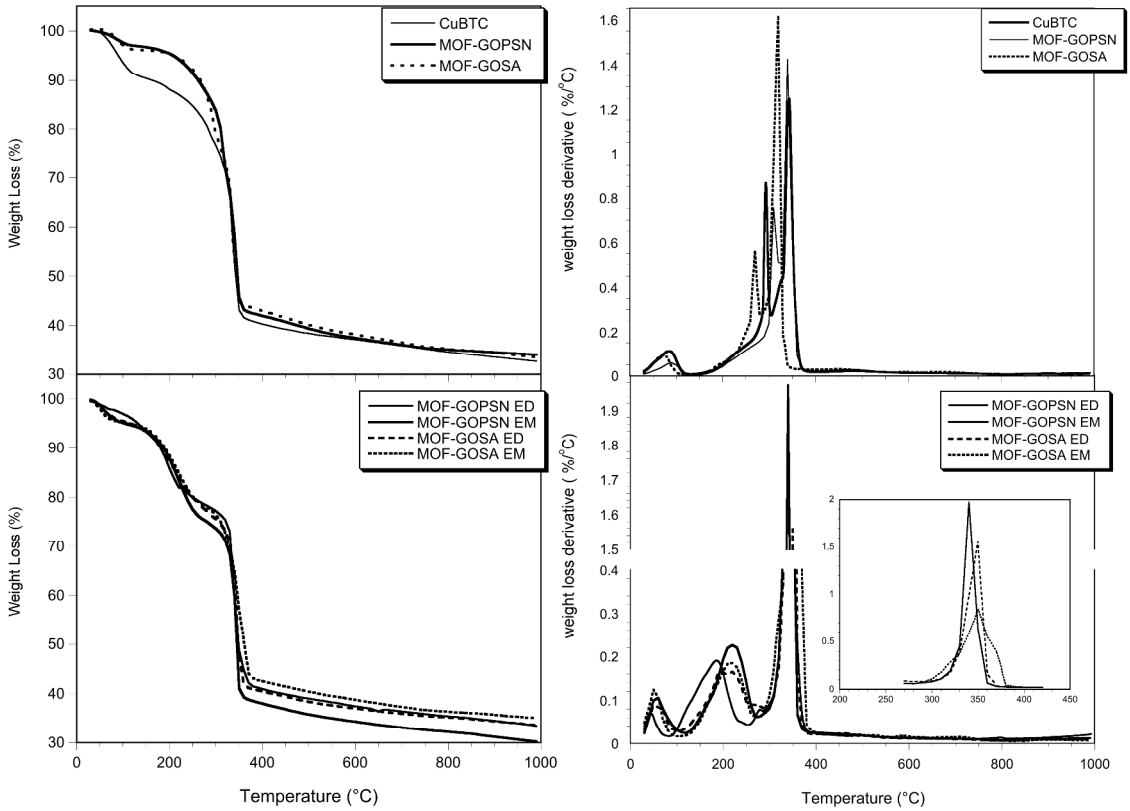

Figure 4.

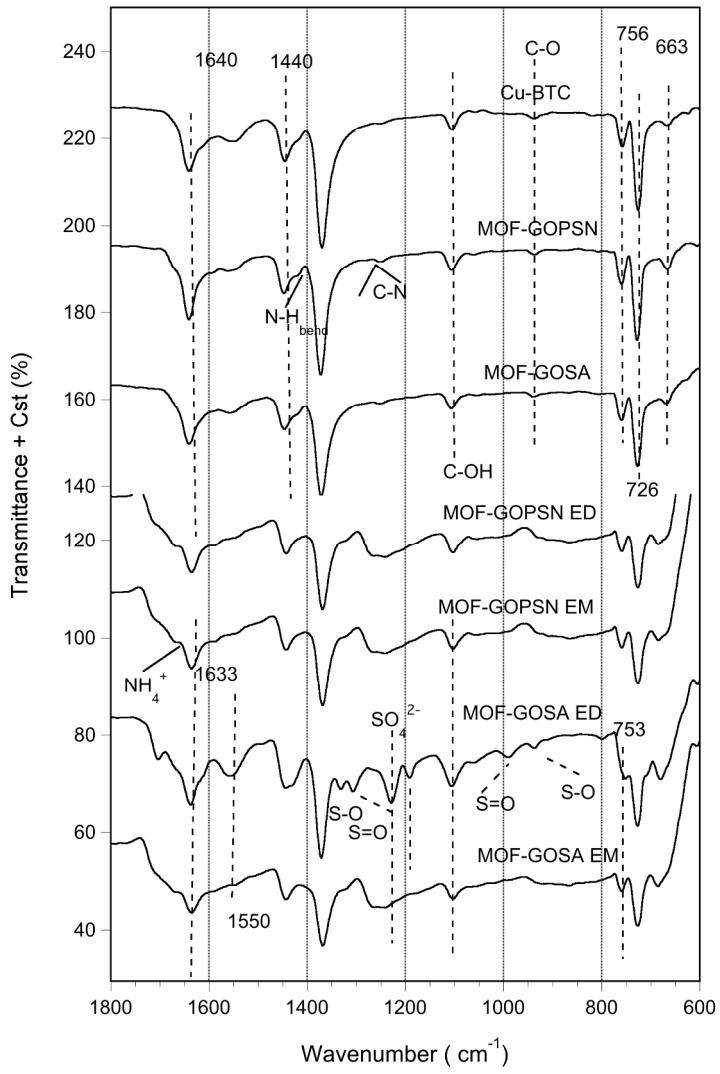

Figure 5.

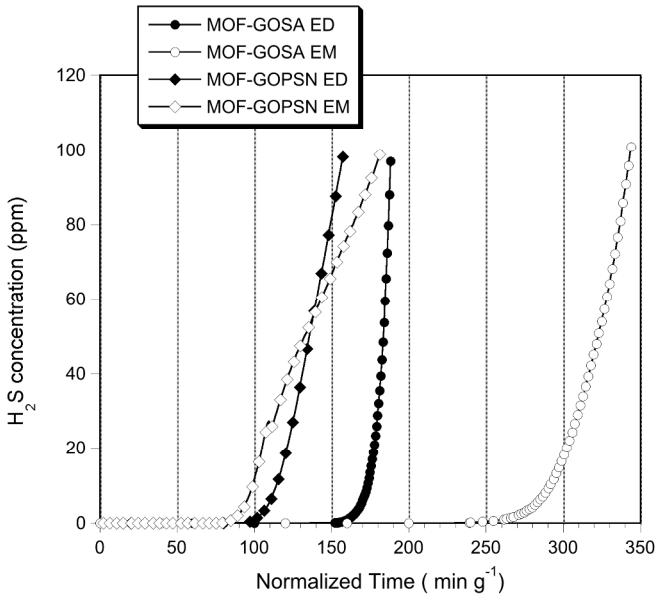

Figure 6.

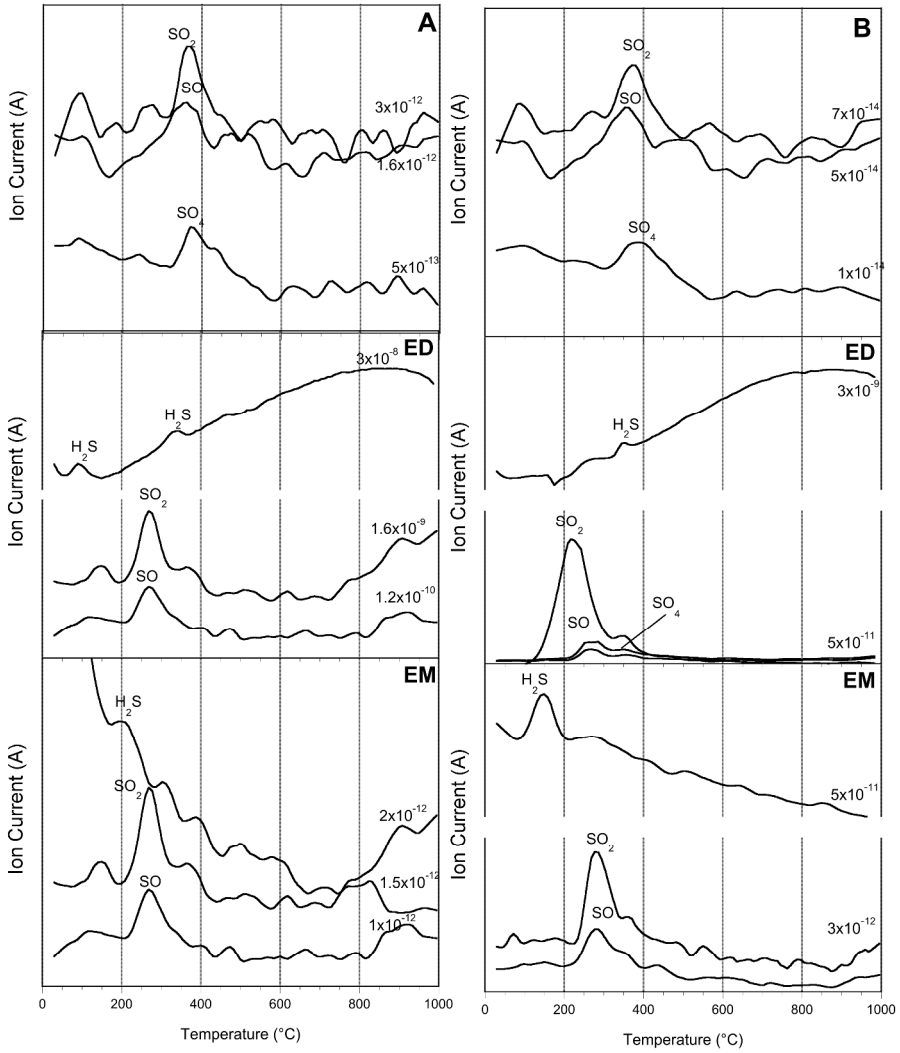

Figure 7.

Table of Contents Entry